A&A 443, 243–250 (2005)
DOI: 10.1051/0004-6361:20053323

Astronomy & Astrophysics

The thermonuclear production of ^{19}F by Wolf-Rayet stars revisited

A. Palacios[1], M. Arnould[1], and G. Meynet[2]

[1] Institut d'Astronomie et d'Astrophysique, Université Libre de Bruxelles, Bd. du Triomphe CP 226, 1050 Brussels, Belgium
e-mail: palacios@astro.ulb.ac.be
[2] Geneva Observatory, 51 Ch. des Maillettes, 1290 Sauverny, Switzerland

Received 27 April 2005 / Accepted 19 July 2005

ABSTRACT

New models of rotating and non-rotating stars are computed for initial masses between 25 and 120 $M_\odot$ and for metallicities $Z = 0.004$, 0.008, 0.020, and 0.040 with the aim of reexamining the wind contribution of Wolf-Rayet (WR) stars to the ^{19}F enrichment of the interstellar medium. Models with an initial rotation velocity $\upsilon_{\rm i} = 300$ km s^{-1} are found to globally eject less ^{19}F than the non-rotating models. We compare our new predictions with those of Meynet & Arnould (2000, A&A, 355, 176), and demonstrate that the ^{19}F yields are very sensitive to the still uncertain $^{19}\mathrm{F}\,(\alpha\,,p)\,^{22}\mathrm{Ne}$ rate and to the adopted mass loss rates. Using the recommended mass loss rate values that take into account the clumping of the WR wind and the NACRE reaction rates, when available, we obtain WR ^{19}F yields that are significantly lower than predicted by Meynet & Arnould (2000, A&A, 355, 176) and that would make WR stars non-important contributors to the galactic ^{19}F budget. In view, however, of the large nuclear and mass loss rate uncertainties, we consider that the question of the WR contribution to the galactic ^{19}F remains quite open.

Key words. stars: interiors – stars: rotation – stars: abundances – nucleosynthesis, nuclear reactions, abundances

1. Introduction

The solar system has for long been the only location in the Universe with a known fluorine (^{19}F) content. The very origin of this ^{19}F has been a major long-standing nucleosynthetic puzzle, in spite of the fact that it has the lowest solar abundance among the nuclides ranging from carbon to calcium.

Since the beginning of the nineties, the situation has changed drastically, both theoretically and observationally. The first quantitative prediction that ^{19}F could be produced thermonuclearly at a level compatible with the solar amount has been made by Goriely et al. (1989). They identify a mode of production of ^{19}F that could develop in He-burning conditions following the reaction chains

$$^{14}\mathrm{N}(\alpha,\gamma)^{18}\mathrm{F} \rightarrow \begin{cases} (\beta^+)^{18}\mathrm{O}(p,\alpha)^{15}\mathrm{N}(\alpha,\gamma)^{19}\mathrm{F} \\ (n,p)^{18}\mathrm{O}(p,\alpha)^{15}\mathrm{N}(\alpha,\gamma)^{19}\mathrm{F}(\alpha,p)^{22}\mathrm{Ne}. \\ (n,\alpha)^{15}\mathrm{N}(\alpha,\gamma)^{19}\mathrm{F} \end{cases}$$

In this scenario, the synthesis of ^{19}F requires the availability of neutrons and/or protons. They are mainly produced by the reactions $^{13}\mathrm{C}\,(\alpha\,,n)\,^{16}\mathrm{O}$ and $^{14}\mathrm{N}\,(n\,,p)\,^{14}\mathrm{C}$.

The viability of the proposed He-burning ^{19}F production scenario has been demonstrated in the framework of detailed models for aymptotic giant branch (AGB) stars (Forestini et al. 1992; Mowlavi et al. 1998; Lugaro et al. 2004), as well as of massive stars evolving through the Wolf-Rayet (WR) stage (Meynet & Arnould 1993, 2000, hereafter Paper I; Stancliffe et al. 2005). Massive stars that do not experience the WR phase are expected to instead produce an insignificant amount of ^{19}F during their hydrostatic evolution (Meynet & Arnould 1993; Woosley & Weaver 1995; Limongi & Chieffi 2003). Note that the Type II supernova explosions of massive stars have also been claimed to be responsible for a ^{19}F production through μ- and τ-neutrino spallation on ^{20}Ne (e.g. Woosley & Weaver 1995). This production is highly uncertain, as it is very sensitive to the poorly known neutrino energy spectra. It will not be discussed here.

The most recent solar and meteoritic ^{19}F values are provided by Lodders (2003) and Asplund et al. (2005). Observational efforts to determine ^{19}F abundances outside the solar system have been largely triggered by the early theoretical predictions of Goriely et al. (1989). In a companion paper to the one of Forestini et al. (1992), Jorissen et al. (1992) provide the first ^{19}F abundances measured in stars other than the Sun. They analyse a number of s-processed enriched galactic MS, S, and N-type giants having a near-solar metallicity. These observations demonstrate that AGB stars are fluorine producers, nicely confirming the initial predictions by Goriely et al. (1989) and Forestini et al. (1992). The derived ^{19}F abundances correlate with the carbon and s-nuclide ones, a pattern that AGB models can also account for, as first shown by Mowlavi et al. (1998). Very recently, ^{19}F has also been detected in a sample of H-rich, as well as H-deficient PG 1159-type hot post-AGB stars

(Werner et al. 2004). The H-rich stars, which are not especially C-rich, show solar-like ^{19}F abundances. This is in line with the conclusion by Jorissen et al. (1992) concerning the C-F correlation in AGB stars. In contrast, the H-poor stars exhibit very large F overabundances ranging from 10 to 250 times solar. Werner et al. (2004) suggest that this abundance pattern might be explained by the operation of a late post-AGB shell flash (see Herwig et al. 1999). As a complement, a F/H abundance ratio of 4.5×10^{-8} has also been determined in a planetary nebula (Liu 1998). This value again agrees with the Jorissen et al. (1992) correlation between F and C.

Fluorine data also exist for stars whose surface, in contrast to the (post-)AGB stars, is not expected to be contaminated with the products of their in-situ nucleosynthesis. This concerns a few near-solar metallicity K and M giants also analysed by Jorissen et al. (1992). In addition, Cunha et al. (2003) have studied a sample of red giant stars in the Large Magellanic Cloud, as well as in the atypical galactic globular cluster ω Centauri. These low-metallicity giants exhibit subsolar fluorine abundances (A(F)[1] $\in$ [3; 4.19]), while both the K–M field giants and the three K–M pre-main sequence low-mass stars of the Orion nebula cluster exhibit nearly solar fluorine (A(F) $\simeq$ 4.55) (Cunha & Smith 2005). This effect of metallicity is in agreement with the general behaviour of [F/O] exhibited by stars in different evolutionary phases within the galactic disk. Such observations of non-contaminated stars spanning a range of metallicities are mandatory if one wants to build a model for the evolution of the ^{19}F content of the Galaxy and of other stellar systems (Renda et al. 2004). Finally, fluorine has also been observed in various interstellar locations (Federman et al. 2004, and references therein) in an attempt to constrain the ^{19}F nucleosynthesis models.

The aim of this paper is to revisit the predictions of Paper I of the ^{19}F yields of WR stars using new models for different masses and metallicities, and to provide the first predictions of ^{19}F production by rotating WR stars.

2. Input physics

The models used here were computed with the Geneva stellar evolution code from the Zero Age Main Sequence (ZAMS) up to the end of the He-burning (HeB) phase, and are listed in Table 1. The physical ingredients, structural predictions, and comparisons to observations are discussed at length by Meynet & Maeder (2003, Figs. 9−12 and Tables 1−2, and 2005, Figs. 7−9 and Tables 1 and 3). The main points of relevance to the ^{19}F synthesis are as follows:

(1) The initial compositions for the different metallicities were selected as in Palacios et al. (2005). The initial ^{19}F mass fraction $X_{19} \equiv X_{19}(Z, 0)$ at metallicity Z was derived from the simple scaling $X_{19}(Z, 0) = (Z/0.02)X_{19\odot}$, where 0.02 is the adopted metallicity for the Sun, and $X_{19\odot} = 4.1 \times 10^{-7}$ is the solar ^{19}F mass fraction according to Grevesse & Noels (1993);

(2) The effect of rotation on the mass loss rate $\dot{M}$ was taken into account following Maeder & Meynet (2001). As reference $\dot{M}$, we adopted for the pre-WR stages the values proposed by Vink et al. (2000, 2001), who account for the occurrence of bi-stability limits which affect the wind properties and mass loss rates. Outside the domain covered by these authors, the rates from de Jager et al. (1988) were selected. As the empirical $\dot{M}$ values was derived from stars with a variety of rotation velocities, and as $\dot{M}$ decreases with these velocities, a reduction factor to the empirical rates of 0.85 (Maeder & Meynet 2001) was introduced for the non-rotating models. During the WR phase, we used the $\dot{M}$ prescriptions of Nugis & Lamers (2000). These rates, which account for the clumping of the winds, are 2 to 3 times smaller than the ones used in previous non-rotating "enhanced mass loss rate" stellar models presented in Paper I. Note that wind anisotropies induced by rotation were neglected. These anisotropies are indeed shown to be very small for the initial velocity $\upsilon_{\rm i} = 300$ km s^{-1} (Meynet & Maeder 2003) selected in this work (see point 6 below). This would not be true for higher initial velocities (Maeder 2002);

(3) During the pre-WR phases, it was assumed that the mass loss rates have a metallicity dependence given by $\dot{M}(Z) = (Z/0.02)^{1/2}\dot{M}(0.02)$ (Kudritzki & Puls 2000; Vink et al. 2001). In contrast, no metallicity dependence was introduced during the WR stage;

(4) All the models were computed with moderate core overshoot. The distance of overshoot was taken equal to $d = \alpha H_{\rm p}$, where $H_{\rm p}$ is the pressure scale height at the Schwarzschild boundary and $\alpha = 0.1$. This value of α is twice as small as the value used in the models of Paper I;

(5) The transport of the nuclides and of the angular momentum was described as in Maeder & Meynet (2001) and Meynet & Maeder (2002) ;

(6) All the considered stars were assumed to rotate on the ZAMS at an initial rate $\upsilon_{\rm i} = 300$ km s^{-1}. For $Z = 0.02$, this value leads to time averaged equatorial velocities on the Main-Sequence (MS), well in the observed range (between 200 and 250 km s^{-1});

(7) The reaction rates adopted in Paper I were updated by the use of the NACRE data (Angulo et al. 1999), when available. The rates of the reactions entering the chain displayed in Sect. 1 that are not considered in NACRE were taken from the following references: ^{14}N $(n\,,p)$ ^{14}C

Table 1. Values of $p_{19}^{\rm wind}(M_{\rm i}, Z)$ in units of 10^{-6} $M_\odot$ for the rotating and non-rotating models also displayed in Fig. 3.

$M(M_\odot)$	$\upsilon_{\rm i}$ (km s^{-1})	$p_{19}^{\rm wind}$ (10^{-6} $M_\odot$)			
		$Z = 0.04$	$Z = 0.02$	$Z = 0.008$	$Z = 0.004$
120	300	5.38	−24.13	18.6	29.1
120	0	51.86	110.05		
85	300	28.41			
60	300	27.97	19.4	−5.18	−1.81
60	0	103.5	22.96		
40	300	27.67		−2.32	−0.757
30	300			−1.49	−0.284
25	300	15.17	−6.03		
25	0	−1.6	−0.201		

[1] A(X) = log [n(X)/n(H)]+12.

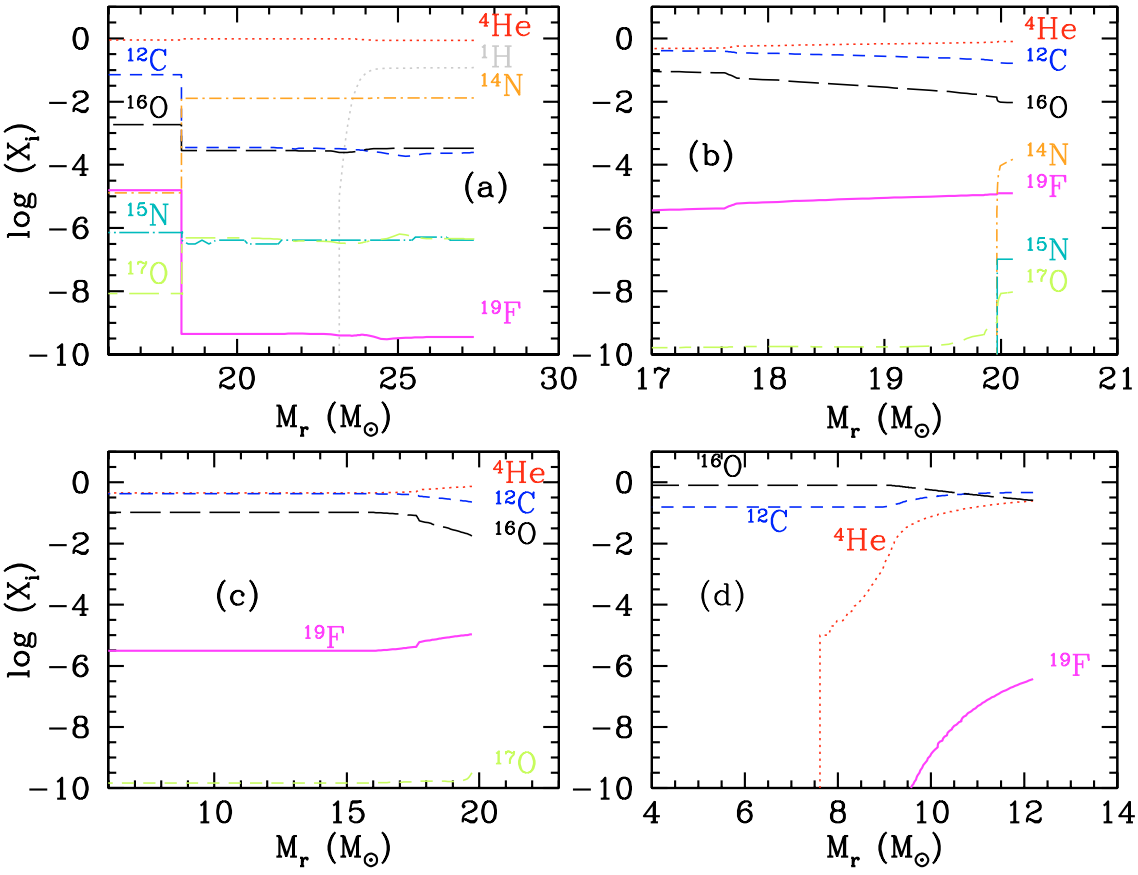

Fig. 1. Mass fractions of the CNO species and of ^{19}F versus mass M_r (in $M_\odot$) inside a 60 $M_\odot$ with metallicity $Z = 0.02$ and $\upsilon_i = 0$ km s^{-1} at three stages during the core He-burning phase (panels **a)–c)**), and at the beginning of core C-burning (panel **d)**). Panel **a)**: X_{19} reaches its maximum value at the centre; **b)**: X_{19} starts to exceed about 10^{-6} at the surface; **c)**: X_{19} reaches its maximum value at the surface; **d)**: there is no more fluorine in the core at the beginning of the C-burning phase.

(Brehm et al. 1988), ^{18}F$(n,p)^{18}$O (REACLIB, Thielemann et al. 1987), ^{18}F$(n,\alpha)^{15}$N (Caughlan & Fowler 1988, hereafter CF88), and ^{19}F$(\alpha,p)^{22}$Ne (CF88).

3. The WR production of ^{19}F

Figure 1 shows the abundances of various nuclides inside the non-rotating 60 $M_\odot$, $Z = 0.02$ model at three stages during the core He-burning (HeB) phase associated with (a) the maximum mass fraction $X_{19,C}$ of fluorine at the centre, (b) the first time the mass fraction $X_{19,S}$ of fluorine at the surface exceeds 10^{-6}, and (c) the maximum mass fraction $X_{19,S}$ of fluorine at the surface. Panel (d) refers to the beginning of the C-burning phase, when there is no fluorine left in the core. We focus on the HeB stage, since ^{19}F is produced in the convective core at the beginning of that phase mainly through the first chain of transformation of ^{14}N into ^{19}F displayed in Sect. 1. In only about 43 300 yrs, while the central He mass fraction $X_{4,C}$ drops from 0.98 to about 0.90, the ^{19}F mass fraction at the centre $X_{19,C}$ is seen to increase from 4.4×10^{-10} to its maximum value 1.6×10^{-5} (see panel (a)). At this time, the surface ^{19}F mass fraction $X_{19,S}$ is still very small (3.6×10^{-10}). As evolution proceeds, the convective core retreats in mass, leaving in its wake ^{19}F-enriched layers that will eventually appear at the surface when the star enters the WC phase (see panels (b) and (c)). The strong wind during this phase finally allows the ejection of these fluorine-rich layers in the interstellar medium (hereafter ISM). Panel (b) depicts the situation when $X_{19,S}$ just exceeds 10^{-6}. The time elapsed between panels (a) and (b) is on the order of 148 000 yrs, corresponding to a $X_{4,C}$ decrease from 0.90 to 0.47. During this period, ^{19}F in the convective core is partly destroyed by ^{19}F$(\alpha,p)^{22}$Ne. In panel (b), $X_{19,C} = 3.7\times10^{-6}$, which is more than 4 times lower than its maximum value. Concomitantly, mass loss starts exposing the most ^{19}F-rich layers at the surface (panel (c)). From this stage on, the synthesised ^{19}F starts enriching the ISM until the outer layers are severely ^{19}F-depleted, as is the case at the beginning of core C-burning (panel (d)).

A generic sequence summarising the above can be used to describe the evolution of the central and surface ^{19}F mass fractions in all the models presented here. Fluorine is produced in the convective core, and its mass fraction rapidly increases at the beginning of the He-burning phase. The regions above the convective core are not ^{19}F -rich at this stage. As the evolution proceeds, the central temperature becomes high enough for ^{19}F$(\alpha,p)^{22}$Ne to be efficient, leading to a decrease of the ^{19}F mass fraction in the convective core. On the other hand, the convective core retreats in mass as a result of strong mass loss. This allows part of the fluorine left behind by the retreating

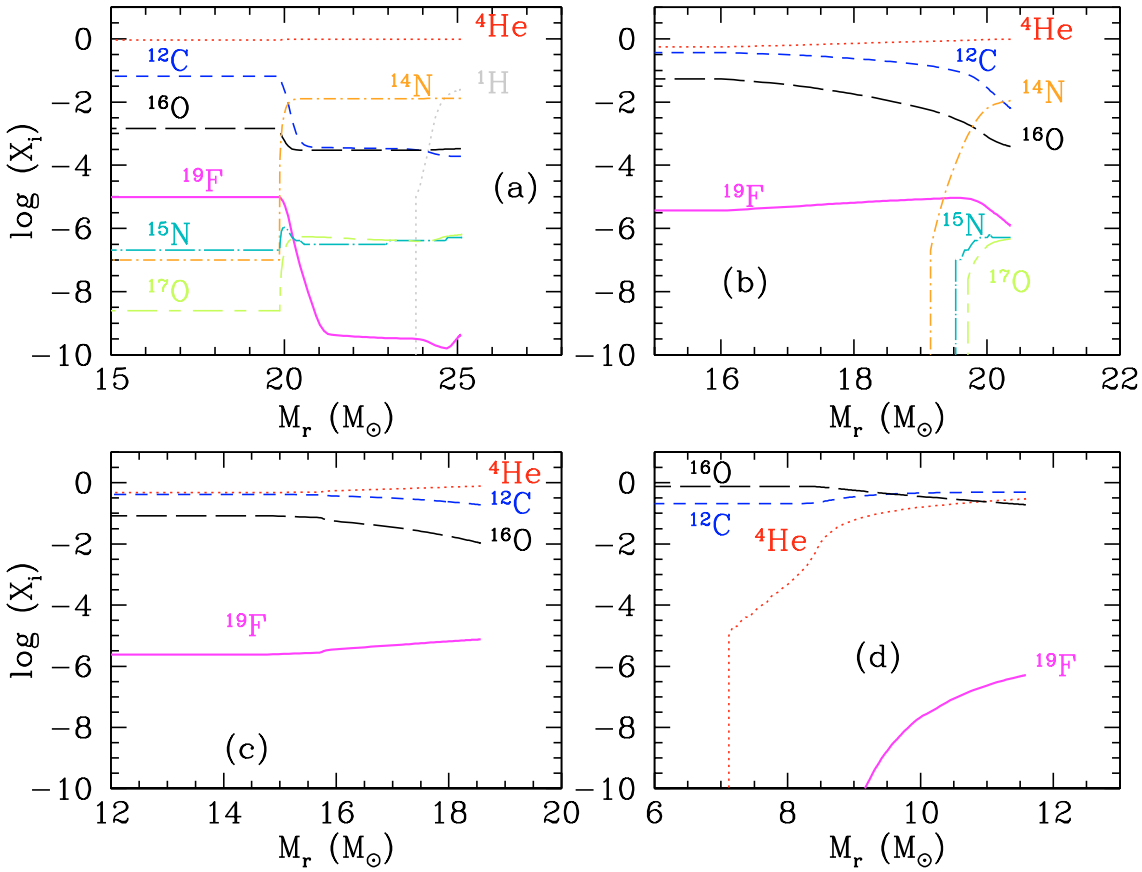

Fig. 2. Same as Fig. 1, but for the $Z = 0.02$ 60 $M_\odot$ model with $\upsilon_i = 300$ km s^{-1}.

core to escape destruction. This fluorine can then be exposed at the surface by the stripping of the outer layers by stellar winds. Thus, at the surface, the ^{19}F mass fraction increases, reaches a maximum, and then decreases as deeper layers are revealed.

From the above, it appears that WR stars can be ^{19}F contributors to the ISM if at least:

(1) The star can enter the WC phase at a sufficiently early phase of core He-burning, so that the ^{19}F -enriched shells of the He-core, which coincide with those rich in carbon and oxygen, can appear at the stellar surface before fluorine is too depleted (see Sect. 3).
(2) The mass loss at the beginning of the WC phase is high enough for efficiently removing the ^{19}F-rich layers. If mass loss is weak at this stage, part of the ^{19}F has time to be converted into ^{22}Ne when deeper layers are uncovered. The fulfilment of these two conditions depends on initial mass, metallicity, and rotation velocity, as discussed below.

The ^{19}F ISM enrichment efficiency of a star with initial mass M_i and metallicity Z, undergoing a wind phase of duration $\tau(M_i, Z)$, is conveniently evaluated in terms of its net ^{19}F yield $p_{19}^{\rm wind}$ defined as

$$p_{19}^{\rm wind}(M_i, Z) = \int_0^{\tau(M_i,Z)} [X_{19,S}(M_i, Z, t) - X_{19,S}(Z, 0)]\dot{M}(M_i, Z, t)\mathrm{d}t. \quad (1)$$

This quantity is a classical input in galactic chemical evolution models. However, it does not represent the total yields of ^{19}F, since more fluorine could be produced during the supernova explosion. Note also that negative $p_{19}^{\rm wind}$ values are obtained when the ejected material contains less ^{19}F than originally present in the star. The yields for the wind phase derived for both our rotating and non-rotating models are displayed in Table 1 in units of 10^{-6} $M_\odot$.

4. Sensitivity of ^{19}F production to initial conditions

4.1. Effect of rotation

Our calculations indicate that rotation has a very limited impact on the ^{19}F production in the stellar cores. This results largely from the fact that rotation hardly affects the temperatures and densities in the core, as well as from the inability of rotation to transport ^{14}N from the H-burning shell into the He core, which would significantly boost ^{19}F production. The insensitivity of the ^{19}F content to rotation for the 60 $M_\odot$, $Z = 0.02$ model is seen from a comparison of Figs. 1 and 2. Let us note that we cannot at this point exclude the possibility of a ^{14}N mixing into the core for rotation velocities and metallicities different from the ones considered here.

The limited role played by rotation on the ^{19}F content of the core does not preclude changes in the ^{19}F yields, as shown in Table 1 and Fig. 3. In fact, $p_{19}^{\rm wind}$ is found in all the considered cases to decrease when rotation is included, except in the 25 $M_\odot$ case at $Z = 0.04$. The magnitude of this reduction shows high sensitivity to mass and metallicity. The $p_{19}^{\rm wind}$

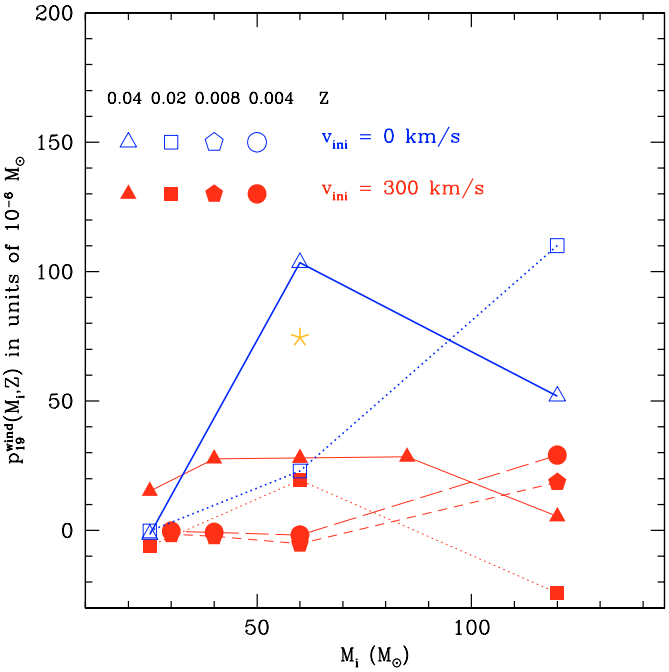

Fig. 3. Values of $p_{19}^{\rm wind}(M_{\rm i},Z)$ in units of 10^{-6} $M_\odot$ for non-rotating (open symbols) or rotating (filled symbols) models with $Z = 0.004$ to 0.04, the different metallicities being represented as indicated in the figure. The black star represents $p_{19}^{\rm wind}(60, 0.02)$ in the non-rotating case, and with the CF88 rate for $^{19}{\rm F}\,(\alpha\,,p)\,^{22}{\rm Ne}$ divided by 10.

lowering with rotation can be explained as follows. Rotation and associated transport processes favour an early entrance of the stars into their WR phase (Fliegner & Langer 1995; Meynet & Maeder 2003). Consequently, the period of high mass loss rate is lengthened, with the result that the rotating models enter their WC phase with, in general, a lower mass. At this stage, the mass loss rate scales with the actual luminosity of the star (Nugis & Lamers 2000), and thus with its actual mass, since the WC stars obey a mass-luminosity relation (Schaerer & Maeder 1992). The mass of the ^{19}F-enriched material ejected into the ISM during the WC phase is thus lowered as a result of rotation. This $p_{19}^{\rm wind}$ reduction appears to be especially limited for the 60 $M_\odot$ model at $Z = 0.02$, due to a balance between different effects acting in this particular case (see also Meynet & Maeder 2003). The non-rotating model enters the WR phase after a short Luminous Blue Variable (LBV) phase characterised by a very high $\dot{M}$, while the WR phase with rotation already starts during the MS, so that the LBV phase is skipped. The short LBV phase experienced by the non-rotating star compensates for its later entry into the WR phase. As a net result, the rotating and non-rotating 60 $M_\odot$ models enter the WC phase with about the same mass. As far as the 25 $M_\odot$, $Z = 0.04$ case is concerned, the rotating star ejects some amount of ^{19}F, while its non-rotating counterpart does not. This derives from the rotating model entering the WC phase, which is not the case in absence of rotation.

In conclusion, mixing induced by rotation does not affect the amount of ^{19}F synthesised in the central regions of the star at the beginning of the core He-burning phase, at least for the range of metallicities explored here. This might not be true any more at very low metallicity, in which case shear mixing appears to be more efficient (Meynet & Maeder 2002). Through structural effects (extent of convective cores, mass-loss enhancement), rotation may however affect the overall evolution of stars during the WR phase in such a way as to modify the $p_{19}^{\rm wind}$ values.

4.2. Effect of mass and metallicity

Stars with different metallicities are likely to produce different amounts of ^{19}F. This is confirmed in Fig. 4 for a rotating 60 $M_\odot$ star. As in the non-rotating models, $X_{19,{\rm C}}$ increases with metallicity (see Paper I). This relates directly to the enhanced production of ^{14}N by the CNO cycles during the central H-burning phase. The larger amount of ^{14}N available at the beginning of the HeB phase allows more ^{19}F to be synthesised. The very limited change of the central densities and temperatures with metallicity does not affect this conclusion. Increased metallicities also favour higher $X_{19,{\rm S}}$ values as a result of higher mass loss rates ($\dot{M} \propto Z^{1/2}$), which allow ^{19}F-enriched layers to be exposed at the stellar surface before the eventual partial transformation of ^{19}F by $^{19}{\rm F}\,(\alpha\,,p)\,^{22}{\rm Ne}$. In contrast, some ^{19}F destruction may be unavoidable at lower metallicities.

These general considerations help in interpreting the trends of the ^{19}F yields with mass and metallicity shown in Fig. 3. Let us just focus here on the models with rotation. For $Z < 0.02$, $p_{19}^{\rm wind} < 0$ for $M_{\rm i} \leq 60$ $M_\odot$. The minimum mass for a rotating star to enter the WC phase is $M_{\rm WC} \approx 25$ and 52 $M_\odot$ at $Z = 0.008$ and 0.004. Below these limits, the stars cannot contribute to the ^{19}F enrichment of the ISM through winds. In the $M_{\rm WC} < M_{\rm i} \leq 60$ $M_\odot$ range, $X_{19,{\rm S}}$ has already dropped below its initial value by the time the He-burning products appear at the surface, leading to negative $p_{19}^{\rm wind}$ values. In contrast, the $M_{\rm i} > 60$ $M_\odot$ stars contribute to the ^{19}F enrichment of the ISM, because enough mass is lost in these cases for uncovering the He core before the destruction of ^{19}F. For the 120 $M_\odot$ model, $p_{19}^{\rm wind}$ is larger at $Z = 0.004$ than at 0.008 because the lower-Z star enters the WC phase with a higher mass (48 instead of 31 $M_\odot$ for Z increasing from 0.004 to 0.008), thus losing more mass at this stage.

The trend discussed above is reverted at $Z = 0.02$. At this metallicity, the 25 $M_\odot$ star only marginally enters the WR phase, and does not contribute to the ISM ^{19}F enrichment. $p_{19}^{\rm wind}$ thus grows from negative values for the 25 $M_\odot$ star to a positive value for the 60 $M_\odot$ model. It then decreases again to a largely negative value at 120 $M_\odot$. For this particular case, the model already enters the WR phase during the MS and loses more than 80% of its mass prior to the HeB phase. These ejecta are not ^{19}F -enriched. When the wind becomes ^{19}F-rich at the beginning of the WC phase, the star has only a small remaining mass and $\dot{M}$ is consequently small from this point on, allowing only a limited amount of ^{19}F-rich material to be ejected. This results in a negative $p_{19}^{\rm wind}$ value.

At $Z = 0.04$, $p_{19}^{\rm wind}$ is positive for all models, and is seen to be rather insensitive to stellar mass. This results from a subtle balance between the dependence with mass of $X_{19,{\rm S}}$ and the amount of ejected ^{19}F-enriched material.

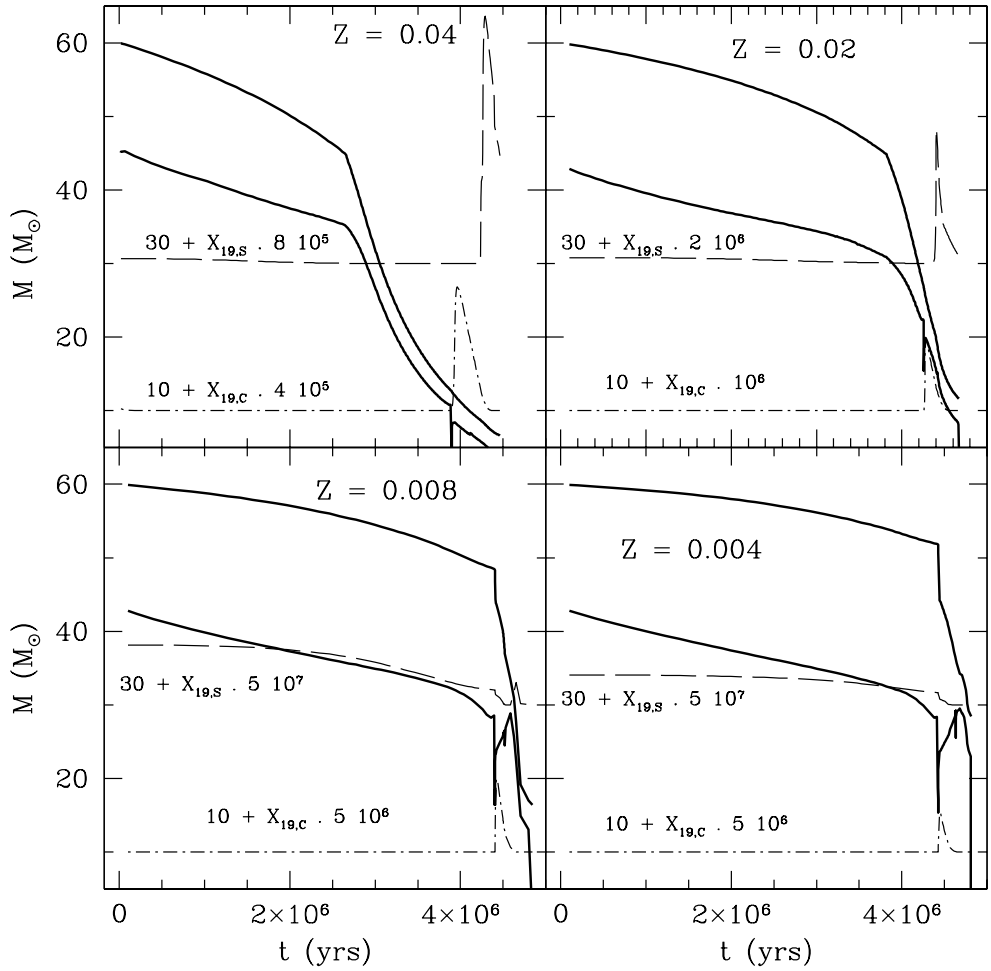

Fig. 4. Evolution of $X_{19,C}$ and $X_{19,S}$ in a 60 $M_\odot$ star with initial rotational velocity υ_i = 300 km s^{-1} at the four indicated metallicities. For display purposes, X_{19} is scaled appropriately. Solid lines describe the evolution of the total and convective core masses.

4.3. Uncertainties in the ^{19}F yields from ^{19}F(α, p)^{22}Ne

The ^{19}F$(\alpha,p)^{22}$Ne reaction is the main ^{19}F destruction channel in the considered stars (see Sect. 1). The large uncertainties on its rate of course concur with the problems of purely astrophysical nature to affect the reliability of the predicted contribution of WR stars to the ^{19}F budget of the Galaxy. The status of our present knowledge of the ^{19}F$(\alpha,p)^{22}$Ne rate has been discussed recently by Lugaro et al. (2004) and Stancliffe et al. (2005). The rate is still poorly known, the uncertainties increasing dramatically with decreasing temperatures. The rate they recommend is more than one order of magnitude smaller than the CF88 rate used in Paper I and in the present work. In view of this, $p_{19}^{\rm wind}$ has been calculated for the 60 $M_\odot$, Z = 0.02 rotating model decreasing the CF88 rate by a factor of 10. As a result, the yield is found to increase by more than a factor of 3, as shown by the black star symbol in Fig. 3. The yield could still be increased slightly by decreasing the rate further. There appears to be room for this, as the lower limit of the rate proposed by Stancliffe et al. (2005) is more than 14 orders of magnitude lower than their recommended rate at $T = 2 \times 10^8$ K! They, however, come to the conclusion that the corresponding yields are only increased by at most 10% if this extremely small lower limit is adopted instead of their recommended rate. This is not surprising, as the yields are essentially "frozen" as soon as the ^{19}F lifetime against α-captures becomes longer than its residence time in He-burning zones. This situation is encountered if the CF88 rate for ^{19}F$(\alpha,p)^{22}$Ne is divided by 2000. Thus, for rates below this limit, $p_{19}^{\rm wind}$ becomes independent of the ^{19}F α-capture rates, and is just some percentage points higher than those displayed in Table 1 and Fig. 3. If ^{19}F$(\alpha,p)^{22}$Ne becomes small enough, one might wonder about other ^{19}F destruction channels, and in particular about the precise role of its radiative neutron captures. In the 60 $M_\odot$ rotating star at Z = 0.02, the mass fraction of neutrons is non-negligible only at the very centre of the star, but decreases rapidly by several orders of magnitude further out in the convective core. Neutron captures are thus not expected to be responsible for a significant destruction of ^{19}F, even if the α-capture channel has reduced efficiency.

5. Comparison with Paper I

Figure 5 is similar to Fig. 3 and presents the yields at Z = 0.02 and 0.04 obtained for the non-rotating models of Paper I and of the present work. The main differences between the two sets of computations lie in the nuclear reaction rates, the amplitude of the core overshoot, and the mass loss prescriptions. For the

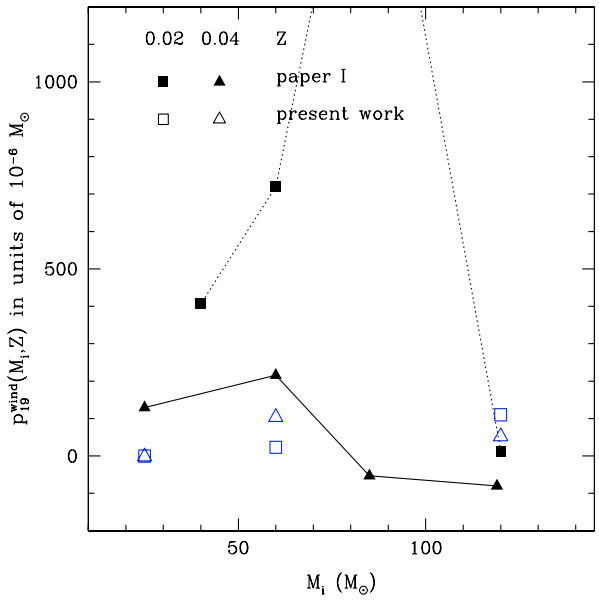

Fig. 5. Same as Fig. 3 for the present non-rotating models (open symbols) and from those of Paper I (filled symbols). Data obtained for $Z = 0.02$ and 0.04 are represented by squares and triangles.

relevant nuclear reactions, the rates adopted here are equal to, or differ only marginally from, the ones used in Paper I, except for ^{15}N(α,γ)^{19}F. The rate from CF88 used in Paper I is replaced by the NACRE (Angulo et al. 1999) adopted one, which is about 34 times smaller than the CF88 one at $T = 2 \times 10^8$ K. However, this change does not affect the ^{19}F production in the non-rotating models. At the beginning of He burning, the α-captures on ^{15}N are very efficient even when adopting the NACRE rate, and ^{15}N is *completely* transformed into ^{19}F well before fluorine starts turning into ^{22}Ne. The net amount of ^{19}F ultimately produced and ejected by WR stars is thus controlled by the destruction channel ^{19}F$(\alpha\,,p)\,^{22}$Ne rather than by the production one.

Concerning the core overshoot its adopted value is lower in the present models than in those of Paper I. All other things being kept the same, we should expect the following consequence of this change. Lower core overshoot leads to smaller He-cores. Smaller He cores imply that more material has to be removed for the core to be uncovered, which clearly disfavours ^{19}F ejection by stellar winds. On the other hand, lower central temperatures result. This does not significantly affect the ^{19}F production from ^{15}N, as ^{15}N anyway has ample time to be totally transformed into ^{19}F. In contrast, the ^{19}F destruction is slowed down, which tends to make its yields greater. Indeed more time is provided to stellar winds to remove the outer layers before fluorine is destroyed in the core. Reduction of the amount of core overshoot should thus have two contrary effects whose relative importance remains unclear.

As already mentioned before, the standard models in Paper I not only differ from the present ones by the core overshoot, but by the adopted mass loss prescription as well, which also modifies the evolution of the core mass and temperature.

Even if this additional difference prevents us from clearly isolating the effect of core overshoot, it appears, however, that the differences with respect to Paper I are dominated by changes in the mass loss prescription. The prescription of Sect. 2 reduces the rates adopted in Paper I by a factor of about 2 to 3. It was emphasised above that the revised prescription has to be preferred, as it takes the clumping of the WR wind into account. In addition, it leads to very good agreement between the observed populations of O-type and WR stars and the predictions relying on rotating models (Meynet & Maeder 2003, 2005).

The impact of a change in the mass loss is intricate, so we try here just to identify general trends. As already mentioned above, for a given star to contribute to the ^{19}F enrichment of the ISM, the mass loss rates have to be high enough at the beginning of HeB to uncover the core before the ^{19}F α-particle captures become efficient enough. From this, one might expect that $p_{19}^{\rm wind}$ increases with increasing mass loss rates at the WC phase. However, as $\dot{M}$ scales with the actual mass during this phase, the removal efficiency of the ^{19}F-rich layers is higher for more massive WC stars, which thus need to have lost a relatively small mass during the previous evolutionary phases. In summary, the WR $p_{19}^{\rm wind}$ yields depend drastically on the mass loss prescriptions. They are high only if the mass loss rates are high enough to remove most of the outer layers at the very beginning of the HeB phase, but low enough for the star to keep a relatively high mass when it enters the WC phase.

The general considerations developed above are confirmed by closer analysis of the non-rotating 60 and 120 $M_\odot$ models. As shown in Fig. 5, the former star is an extreme illustration of the cases for which the present models predict $p_{19}^{\rm wind}$ values lower than those reported in Paper I, with a reduction larger than a factor of about 30. Even if, as made plausible by the discussion above, the differences in the predicted yields likely result from the combined (and difficult to disentangle) effects of the various changes in the ingredients of the two sets of stellar models, the revised mass loss rates are most probably responsible for the new situation encountered for the 60 $M_\odot$ model. The Paper I 60 $M_\odot$ model at $Z = 0.02$ indeed enters the WC phase with a mass of about 24 $M_\odot$ and $X_{4,\rm C} = 0.79$. Only less than 5 $M_\odot$ remain at the end of the evolution. The newly computed model enters the WC phase with a mass of about 21 $M_\odot$. This mass is close to the one computed in Paper I, but is reached later in the evolution, at a point where $X_{4,\rm C} = 0.47$. This delay is of course the direct result of the lower mass loss rates adopted here in the previous phase. In addition, the final mass of the star is 12.4 $M_\odot$. In other words, only 8.6 $M_\odot$ is lost during the WC phase, which is less than half of what is computed in Paper I. All these effects tend to reduce $p_{19}^{\rm wind}$.

In contrast to the situation characterising the $M \leq 60\ M_\odot$ models, the new ^{19}F yields for the non-rotating 120 $M_\odot$ model are higher than those of Paper I (Fig. 5). In Paper I, the star was predicted to lose so much mass that it enters the WC phase with only about 6 $M_\odot$. Just a small amount of material can thus be lost during this phase (as $\dot{M} \propto M$ at this phase). This clearly prevents any high ^{19}F yield. With the new lower $\dot{M}$ values, the same star enters the WC phase with a mass larger than 43 $M_\odot$, and more than 27 $M_\odot$ are lost during the WC phase. This favours higher ^{19}F yields.

6. Conclusions

Revised ^{19}F yields from non-rotating WR stars and the first evaluation of the yields from rotating such stars are presented. The new yields, in the absence of rotation, are significantly lower than those of Paper I, as illustrated by the $Z = 0.02$ 60 $M_{\odot}$ case, where the reduction amounts to more than a factor of 30. Rotation does not help in this matter, and even reduces the yields. This drastic decrease of the predicted ^{19}F yields mainly results from the adoption of reduced mass loss rates and, to a lesser, extent from the selection of a smaller core overshoot.

Taken at face value, these new predictions discard WR stars as important sources of the galactic ^{19}F. Let us, however, emphasise that they suffer from uncertainties originating from at least two sources. As discussed above, $p_{19}^{\rm wind}$ is very sensitive to (1) the still poorly known ^{19}F$(\alpha\,,p)\,^{22}$Ne rate (see also Stancliffe et al. 2005), (2) the still uncertain wind mass loss rates. Interestingly, Meynet & Maeder (2005), on the basis of arguments concerning the WR population at solar and higher than solar metallicities, suggest that the mass loss rates during the post-core H-burning WNL phase might be underestimated. Higher mass loss rates during this short stage would uncover the He-core more rapidly and would likely favour the ejection of ^{19}F.

All in all, we consider that the question of the contribution of WR stars to the galactic ^{19}F remains largely open. It appears reasonable at this point to refrain from drawing any far-reaching conclusion based on the present WR yield predictions, particularly in attempts to build galactic chemical evolution models.

Acknowledgements. A.P. acknowledges financial support from the ESA PRODEX contract 96009.

References

Angulo, C., Arnould, M., Rayet, M., et al. 1999, Nucl. Phys., A656, 3 (NACRE)
Asplund, M., Grevesse, N., & Sauval, A. J. 2005, in Cosmic Abundances as Records of Stellar Evolution and Nucleosynthesis, ed. F. N. Bash, & T. G. Barnes, ASP Conf. Ser., 336
Brehm, K., Becker, H. W., Rolfs, C., et al. 1988, Z. Phys., A330, 167
Caughlan, G. R. & Fowler, W. A. 1988, At. Data and Nuc. Data Tables, 40, 283 (CF88)
Cunha, K, & Smith, V. V. 2005, ApJ, 626, 425
Cunha, C., Smith, V. V., Lambert, D. L., & Hinkle K. H. 2003, AJ, 126, 1305
de Jager, C., Nieuwenhuijzen, H., & van der Hucht, K. A. 1988, A&AS, 72, 259
Federman, S. R., Sheffer, Y., Lambert, D. L., & Smith, V. V., 2005, ApJ, 619, 814
Fliegner, J., & Langer, N. 1995. in IAU Symp., ed. K. A. van der Hucht & P. M. Williams (Dordrecht: Kluwer), 163, 326
Forestini, M., Goriely, S., Jorissen, A., & Arnould, M. 1992, A&A 261, 157
Goriely, S., Jorissen, A., Arnould, M. 1989, in Proc. 5th Workshop on Nuclear Astrophysics, ed. W. Hillebrandt, & E. Müller (Munich: Max-Planck-Institut für Astrophysik Report), 60
Grevesse, N., & Noels, A. 1993, Phys. Scr., 47, 133
Herwig, F., Blöcker, T., Langer, N., & Driebe, T. 1999, A&A, 349, L5
Jorissen, A., Smith, V. V., & Lambert, D. L. 1992, A&A, 261, 164
Kudritzki, R.-P., & Puls, P. 2000, ARA&A, 38, 613
Limongi, M., Chieffi, A. 2003, ApJ, 592, 404
Liu, X.-W. 1998, MNRAS, 295, 699
Lugaro, M., Ugalde, C., Karakas, A. I., et al. 2004, ApJ, 615, 934
Lodders, K. 2003, ApJ, 591, 1220
Maeder, A. 2002, A&A, 392, 575
Maeder, A., & Meynet, G. 2001, A&A, 373, 555
Meynet, G., & Arnould, M. 1993, in Nuclei in the Cosmos II, ed. F. Käppeler, & K. Wisshak (Bristol: IOP), 503
Meynet, G., & Arnould, M. 2000, A&A, 355, 176 (Paper I)
Meynet, G., & Maeder, A. 2002, A&A, 390, 561
Meynet, G., & Maeder, A. 2003, A&A, 404, 975
Meynet, G., & Maeder, A. 2005, A&A, 429, 581
Mowlavi, N., Jorissen, A., & Arnould, M. 1998, A&A, 334, 153
Nugis, T., & Lamers, H. J. G. L. M. 2000, A&A, 360, 227
Palacios, A., Meynet G., Vuissoz C., et al. 2005, A&A, 429, 613
Renda, A., Fenner, Y., Gibson, B. K., et al. 2004, MNRAS, 354, 575
Schaerer, D., & Maeder, A. 1992, A&A, 263, 129
Stancliffe, R. J., Lugaro, M., Ugalde, C., et al. 2005, MNRAS, 360, 375
Thielemann, F.-K., Arnould, M., Truran, J. W., 1987, Adv. in Nucl. Astrophysics, ed. E. Vangioni-Flam, J. Audouze, M. Casse, J.-P. Chieze, & J. Tran Thanh Van (Gif-sur-Yvette: Éditions Frontières), 525
Vink, J. S., de Koter, A. & Lamers, H. J. G. L. M. 2000, A&A, 362, 295
Vink, J. S., de Koter, A. & Lamers, H. J. G. L. M. 2001, A&A, 369, 574
Werner, K., Rauch, T., & Kruk, J. W. 2005, A&A, 433, 641
Woosley, S. E., & Weaver, T. A. 1995, ApJS, 101, 181